Characterization of low cost high-altitude balloons as a near-space testing platform

Matteo Gemignani
Aerospace Division, Dept. of Civil and Industrial Engineering, University of Pisa, Italy
matteo.gemignani6@gmail.com

ABSTRACT

The aerospace industry is currently growing at a fast pace. Differently from what happened in the recent past, space is increasingly seen as a business in which to invest. This has meant that more and more private companies became interested in taking part into this market. Despite this, the space sector still requires big investments. For this reason, in recent years the interest in cheaper solutions has considerably increased.

Following this principle, the main goal of the work here reported was to create a low-cost near-space platform for experimenting and testing on space hardware. The idea is to use the most common type of high-altitude balloon, i.e. sounding balloons, which are nowadays available at very low cost from commercial vendors and freely operable. This because they represent a simple, quick and economical way to launch a payload in a near space environment. Other kind of balloons, such as zero-pressure and super-pressure balloons, widely used by space agencies for science research, are much more expensive and require a large infrastructure to be launched.

This paper presents an application of this concept to the problem of measuring electromagnetic noise in the ISM bands (900 MHz and 2.4 GHz) in the operational environment of a LEO constellation dedicated to IoT telecommunications. We report the design phase, the operative mission phase, and finally discuss the data collected throughout a fully successful campaign of five launches.

1 INTRODUCTION - THE ISM-HAB PROJECT

High-altitude balloons (HAB) have a large potential as hosting vehicles for space hardware experiments. In 2018, Eutelsat tasked the Italian company MBI to investigate the levels of noise in the ISM (Industrial, Scientific, and Medical) bands at orbital altitude while investigating on the feasibility of a LEO constellation [1]. HAB was identified as a quick, low cost platform to bring the measurement hardware to a near-space environment.

Due to its unlicensed nature, the popularity of ISM bands is growing very fast. Nowadays they are worldwide used to operate wireless data links using short-range wireless devices, such as the familiar Wi-Fi domestic appliances. Recently, these bands have been also adopted by several terrestrial operators to deploy Internt-of-Things (IoT) networks over a geographical area using Low Power WAN (LP-WAN) protocols such as Lora [2] and SIGFOX [3] that are using the ISM sub-GHz frequency bands (868 MHz in Europe and 900 MHz in USA).

Figure 1 - ISM-HAB sounding balloon

Moreover, in the recent years several studies aiming at defining new IoT protocols suitable for the satellite environment have been started as well as several attempts to adapt existing terrestrial technologies to the satellite means. The possibility to use portions of the terrestrial ISM bands for telecommunication between the ground terminals and the satellite is very attractive and represent a potential disruptive factor for the next developments of satellite-based IoT networks. However, as result of the popularity growth, the number of devices operating in these bands is rapidly increasing, thus creating an even more congested frequency spectrum that could degrade communication performance. In this scenario, the ISM-HAB project comes into play: thanks to the ease and cost effectiveness of using sounding balloons, it was possible to launch a total number of 5 balloons up to the altitude of 32 km to collect RF power measurements in the ISM bands. At such altitude, the signal was collected from sources scattered over a very large portion of Earth, thus emulating what would be experienced by a LEO satellite.
The levels of interference where measured within the following bands:

- S bands (ISM 2.4 GHz): 2400 – 2483 MHz (83 MHz bandwidth)
- UHF bands (ISM 868 MHz and 900 MHz bands): 862 – 922 MHz (60 MHz bandwidth)

Along with the primary objective of RF noise neasurement, the project offered an excellent opportunity to perform the characterization of the dynamic environment of the HAB platform, in view of the future use of such system for space hardware testing.

2 MISSION DESIGN

The main component of ISM-HAB is a commercial 1.2 kg unmanned high-altitude balloon, made of latex and filled with helium. The balloon is released from the ground into the stratosphere, generally attaining a height between 18 to 37 km (the maximum altitude reached during the ISM-HAB missions is 32 km). The amount of helium is calculated in order to have a specific lift at ground level so to carry the balloon up to the desired altitude. As it ascends through the Earth's atmosphere with a typical speed of 3-5 m/s, the balloon expands up to a certain maximum size, until it eventually bursts because of structural failure of the latex membrane. Figure 3 shows the moment of bursting as captured by one of the onboard cameras on one of our flights.

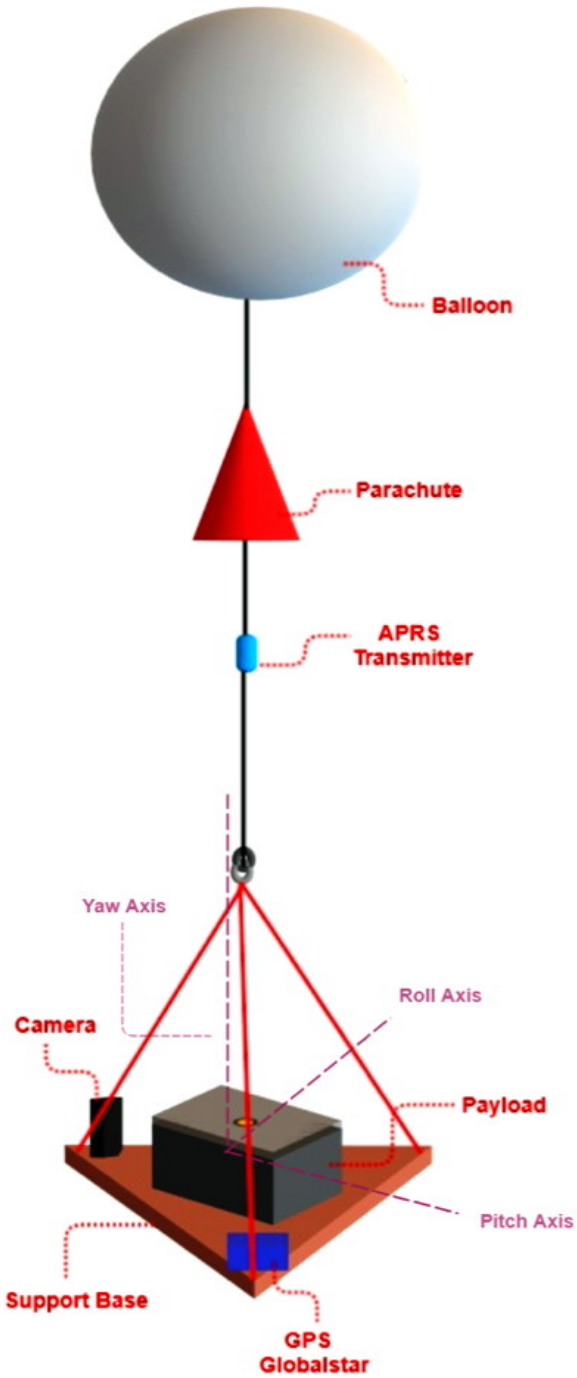

Figure 2 - Main parts of a HAB.

The balloon can carry a group of objects to near space. The objects that are attached to the balloon are often referred to as the "payload train" where each payload serves a particular purpose (Fig. 2). In ISM-HAB the train includes a 1.5 m diameter parachute, a radar reflector and the custom payload designed to perform the ISM measurements, which also includes tracking devices, sensors, and one or more cameras. After the burst, the payload train starts freefalling until the parachute is fully opened, and the descent speed reaches the limit (typically 4-5 m/s) imposed by the size of the parachute and by the attached mass.

Figure 3 – Burst of the balloon

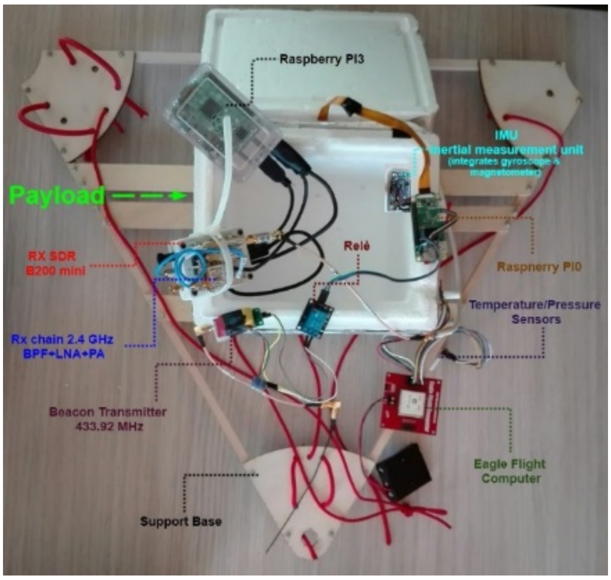

Figure 4 – Sub components inside the styrofoam box

The payload of the HAB is composed of the following main systems:

- The **tracking payload** that is used to track the HAB and to collect data from the on-board sensors. The tracking payloads is composed of several independent sub-systems (see below).
- The **RF payload** that is used to perform the measurement of the aggregated RF power received over the addressed bands while the HAB is flying.

Some components of the payloads are attached directly on the wooden support base, such as the SPOT Globalstar modem, the cameras, the external sensor of the on-board computer and the RX antenna of the RF payload. All other components are installed within a styrofoam box (Fig. 4), the only exception being the ARPS Transmitter that is attached to the cord connecting the parachute to the box. APRS (Automatic Packet Reporting System)

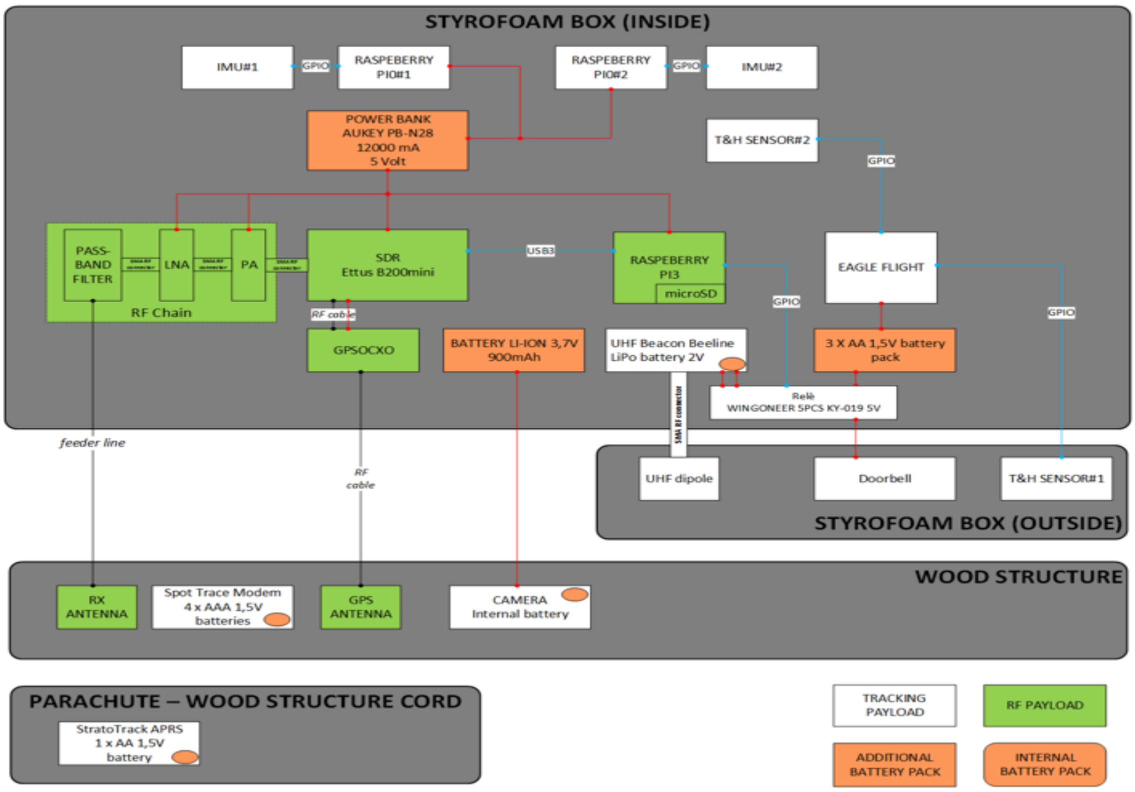

Figure 5 - RF and Tracking payload scheme

is a standard protocol mostly used by radio amateur operators to broadcast GNSS-based location data and other information.

The active components are powered by means of standard power banks (Aukey PB-N28 [4], mainly used to power the RF payload, and LI-ION 3.7 V used to extend the life time of the internal battery of the camera) and battery packs with AA batteries, as shown in Figure 5. This architecture is able to power all the components for more than 4-5 hours, that is the typical duration of a mission.

2.1 Tracking payload

The tracking payload is composed of several sub-systems. Most of them act in a redundant way to maximize the possibility to recover the payload. The sub-systems are listed below.

- The **APRS transmitter** [5], namely the StratoTrack model by StratoGear [6], that is used to transmit every few minutes (three available TX periods of 1.5 to 15 minutes) the position of the HAB collected by the GPS modules embedded in the module, as well as a few additional pieces of information such as the external temperature, GPS lock quality and voltage of its battery pack (Figure 6). The data transmitted using the dedicated VHF channel (144.80 MHz), is collected on ground by one or more of the many existing amateur-operated APRS receiving stations. Data are finally redirected on the internet and can be accessed using the APRS public site (https://aprs.fi).

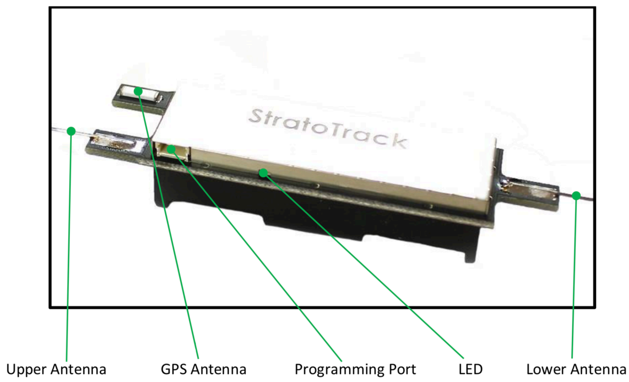

Figure 6 – The APRS transmitter

- The **SPOT Trace Modem** [7] transmits the position of the HAB using the Globalstar LEO constellation every few minutes (Fig. 7). The service is very reliable thanks to the ability of the modem to perform successfully transmissions even if the payload lands deep in the woodlands (in our project, this happened 4 times out of 5).

Figure 7 - The SPOT Trace Modem

- The **on-board computer**, namely the Eagle Flight model by High Altitude Science (HAS) [8], that collects data with a periodicity of 6 s from its embedded GPS receivers as well as from its own two temperature and pressure sensors (Fig. 8). One sensor is installed outdoor in order to record the external temperature and pressure while the second one is located within the styrofoam box.

Figure 8 - The EAGLE fligh computer

- The **Inertial Measurement Unit (IMU)** based on a LSM9DS1 sensor [9] that contains a MEMS accelerometer and a MEMS gyro in a single chip (Fig. 9). Each mission is equipped with one or two LSM9DS1 sensors. This is the key sensor for dynamical characterization, as it provides information about the mechanical oscillations of the payload assembly. Each sensor is controlled by a dedicated Raspberry Pi Zero, which stores the collected data in a microSD memory card [10].

Figure 9 – The Inertial Measurement Unit

- The **UHF Beacon,** namely a BeeLine Transmitter (Fig. 10), that is used to transmit a beacon on 433 MHz used to locate the landed HAB using a UHF Fox Hunter. Considering that the signal cannot be emitted while flying the UHF beacon is activated at landing, using a relay controlled by the Raspberry PI3.

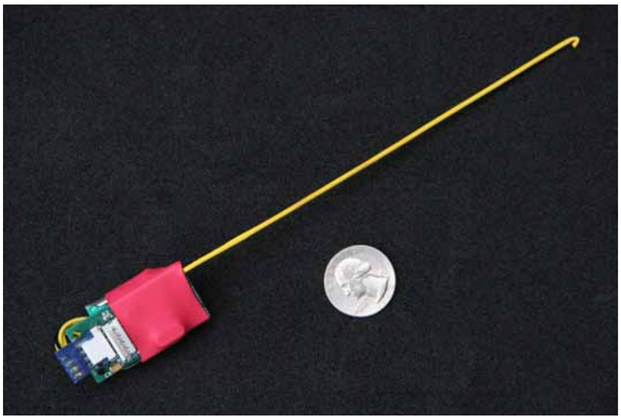

Figure 10 – The BeeLine transmitter

- The 433 MHz controlled **Doorbell** that is used to emit a sound to help recovery of the landed payload during the night or within woodlands.
- The **video camera** used to record a video during the flight. The position of the video camera was changed before every mission in order to adjust the view or to image in different directions.

2.2 RF Payload

All the hardware components used to integrate the RF payload are Commercial-Off-The-Shelf. The on-board antenna, the pass-band filter and the LNA (Low Noise Amplifier) are tuned on UHF or S bands, while the power amplifier, the SDR (Software-Defined Radio) device and the Raspberry PI3 are common to both bands. A GPS OCXO (Oven Controlled Crystal Oscillator) has been added to ISM-HAB#5 in order to increase the frequency stability of the SDR oscillator during the sample recording.

The S-band patch antenna (SMA connector) is attached to base of the payload while the UHF dipole antenna (N connector) is installed parallel to the base at a distance of 7 cm using a plastic bracket in order to maximize the antenna gain (Fig. 11). Both antennas are connected to the pass-band filter with a short SMA coaxial cable (the antenna feeder link).

Figure 11 – S-band antenna (top); UHF antenna (bottom)

All other components of the RF payload apart from the RX antennas, the feeder link and the GPS antenna of the GPS OCXO are installed within a common styrofoam box (20 x 24 x 15 cm) in order to keep the components warm during the flight. The pass-band filter, the LNA, the PA and the SDR device are connected each other using their SMA connectors. Finally, the SDR device is connected to the Raspberry PI3 using a USB cable. The Raspberry PI3 stores the collected data within its micro SD. The diagram in Figure 12 shows the architecture of the RF payload.

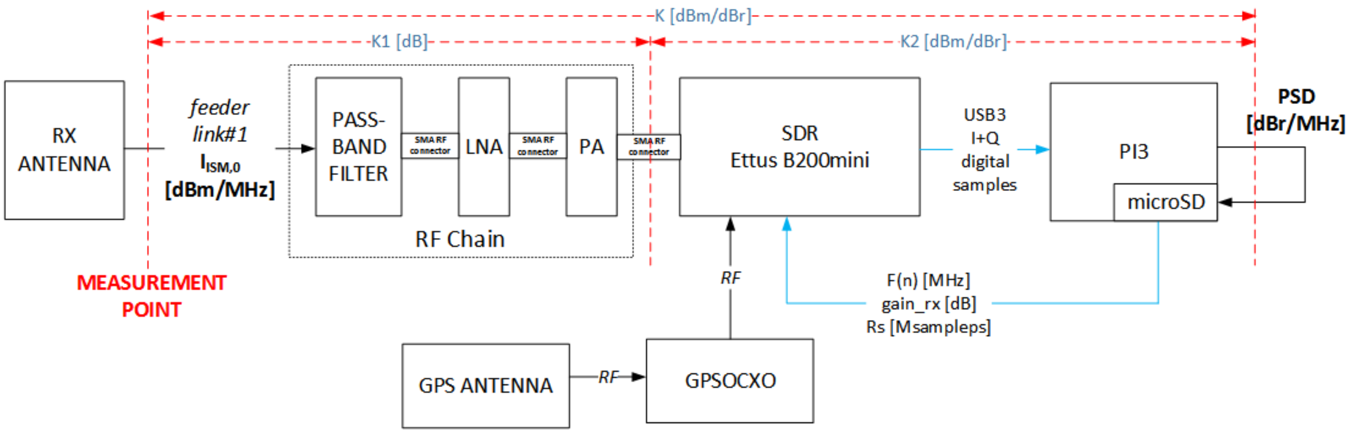

Figure 12 - RF payload architecture

3 MISSION OPERATIONS

Flight Predictions

The useful data that the payload measures during the mission are stored into a micro SD memory card and cannot be transmitted while flying due to their size. Therefore, recovery of the payload is mandatory for the mission success. A large percentage of the success of a mission based on high altitude balloons relies in a precise prediction of the flight path. This because weather conditions, direction and strength of the winds change at almost all times, and knowing in advance the location of the landing site with a sufficient accuracy may be critical to avoid ending up in deep woods or water. All the existing landing predictors are based on calculation of the vertical and horizontal motion and provide the landing site and the flight time as output [11].

3.1 The MBI PyLanding predictor

A custom landing predictor has been developed during this project in order to have a reliable prediction of the flying path. The predictor, written in Python code, can be adjusted to fit different flight conditions, like flight in rainy conditions that typically are not accounted for by predictors available online. The code models independently the ascent and the horizontal motion [12, 13, 14, 15] and uses data provided by NOAA GFS, to be manually imported [16].

3.1.1 Modeling of the ascent

In modeling the flight dynamics of the balloon, there are three forces that are of interest: gravity, buoyancy, and drag. The buoyant force is equal to the magnitude of the weight of the air displaced by the balloon. Since lifting gases are by definition less dense than air, the buoyant force exceeds the force of gravity and propels the balloon upward. The buoyant force, which acts in the *z* direction, is:

$$\vec{F_b}(z) = V(z)\,\rho_{air}(z)\,g(z)\,\hat{z}$$

where *V(z)* is the balloon volume. Latex balloons can expand to a multiple of their launch site diameter at apogee, and the density ρ_{air} of the atmosphere at typical burst altitudes can approach 1% of sea-level density while variations of the gravity acceleration *g(z)* are less than 1-2%. The buoyant force is opposed by the downward force of gravity on the balloon:

$$\vec{F_g}(z) = -\,m_{tot}\,g(z)\,\hat{z}$$

where $m_{tot} = m_{balloon} + m_{payload} + m_{Helium}$ is the mass of the whole system.

Finally, the drag force can be computed as follows:

$$\vec{F_d}(z) = -\,\frac{1}{2}\,\rho_{air}(z)\,C_D\,A(z)\,|V_{rel}|\,\vec{V}_{rel}$$

where:

$$\vec{V}_{rel} = \vec{V} - \vec{V}_W$$

is the balloon's velocity relative to the surrounding air, C_D is the drag coefficient and $A(z)$ is the cross-sectional area of the balloon in the direction of $\vec{V}_{rel}$. The total force acting on the balloon is then:

$$\vec{F_t}(z) = [V(z)\,\rho_{air}(z) - m_{tot}]\;g(z)\,\hat{z} - \frac{1}{2}\,\rho_{air}(z)\,C_D\,A(z)\,|V_{rel}|\,\vec{V}_{rel}$$

The vertical motion is then derived by integrating the total force using Newton's law and imposing the initial conditions and the burst conditions. Two burst conditions can be set, i.e. either the burst altitude, or the burst diameter of the balloon as provided by the manufacturer.

3.1.2 Modeling of the horizontal motion

The horizontal motion is modelled assuming that the x and y components of the HAB velocity are equal to the x and y components of winds. The x component is that parallel to the local parallel while the y one is parallel to the local meridian. These winds components, often referred to as U_v and U_u, are provided by several entities such NOAA for any location in the world with resolution of 1° or 0.5°.

Assuming that Δ_t is the integration time used by the simulator, the horizontal displacements can be computed as follow:

$$\Delta_x = V_{x,W}\,\Delta_t$$
$$\Delta_y = V_{y,W}\,\Delta_t$$

while the variation of the longitude and latitude are:

$$\Delta_{lat} = \operatorname{asin}\left(\frac{V_{y,W}\,\Delta_t}{r_e}\right)$$

$$\Delta_{long} = \operatorname{asin}\left(\frac{V_{y,W}\,\Delta_t}{r_e\,\cos\,(lat)}\right)$$

where $r_e\,\cos(lat)$ is the radius of the circle relative to the parallel with the considered latitude.

3.1.3 Validation of the PyLanding Predictor

The predictor turned out to be very accurate if precisely tuned, as shown in the next table that shows the distance of the predicted landing sites from the actual ones.

Mission	HAB#1	HAB#2	HAB#3	HAB#4	HAB#5
Landing sites distance[km] [%]	1.2 km, 14%	5 km, 6%	2.9 km, 10 %	8 km, 5,83%	3 km, 4 % -

Table 1 –Error between predicted and actual landing sites

Figure 12 shows the simulated trajectory and the real trajectory in a typical fligh case.

The results of the PyLanding predictor are quite accurate and very satisfacory. However, the simulator is still open to further devlopment, e.g. by including thermal effects such as solar radiation heating and by adding a graphical interface that simplifies the interaction with the user.

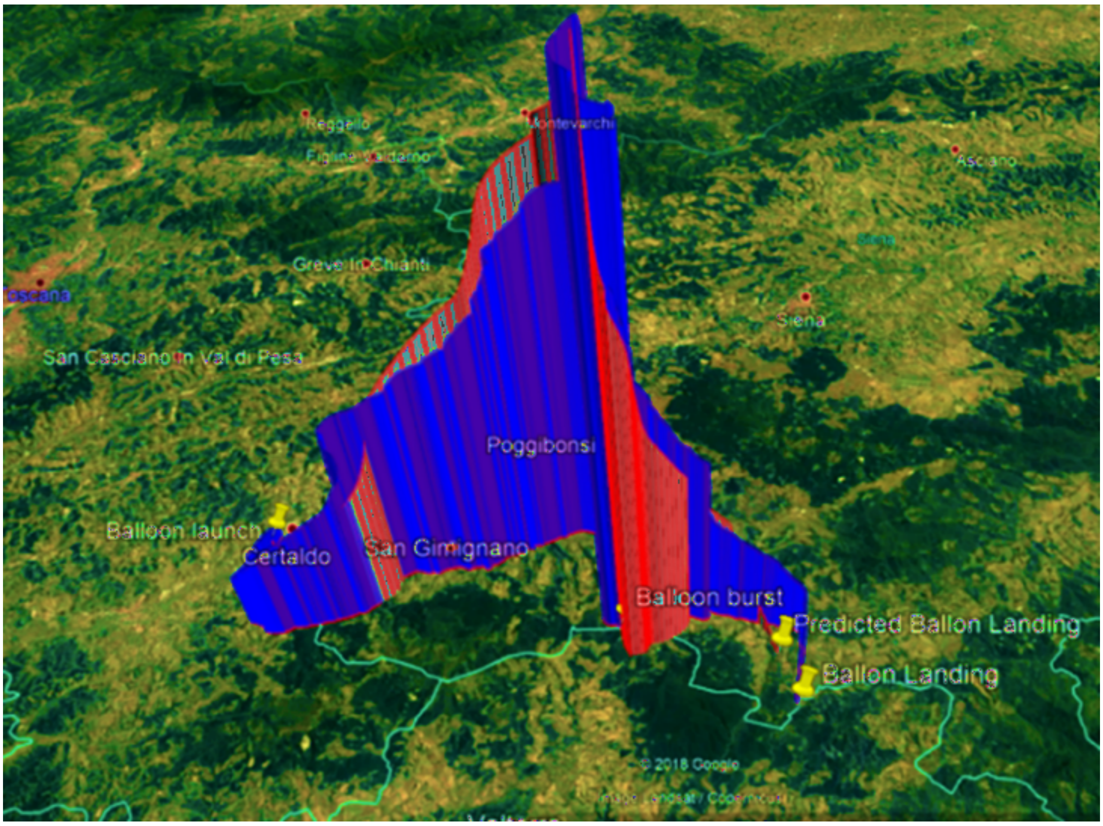

Figure 12 - Simulated trajectory (red) vs. real tralectory (blue)

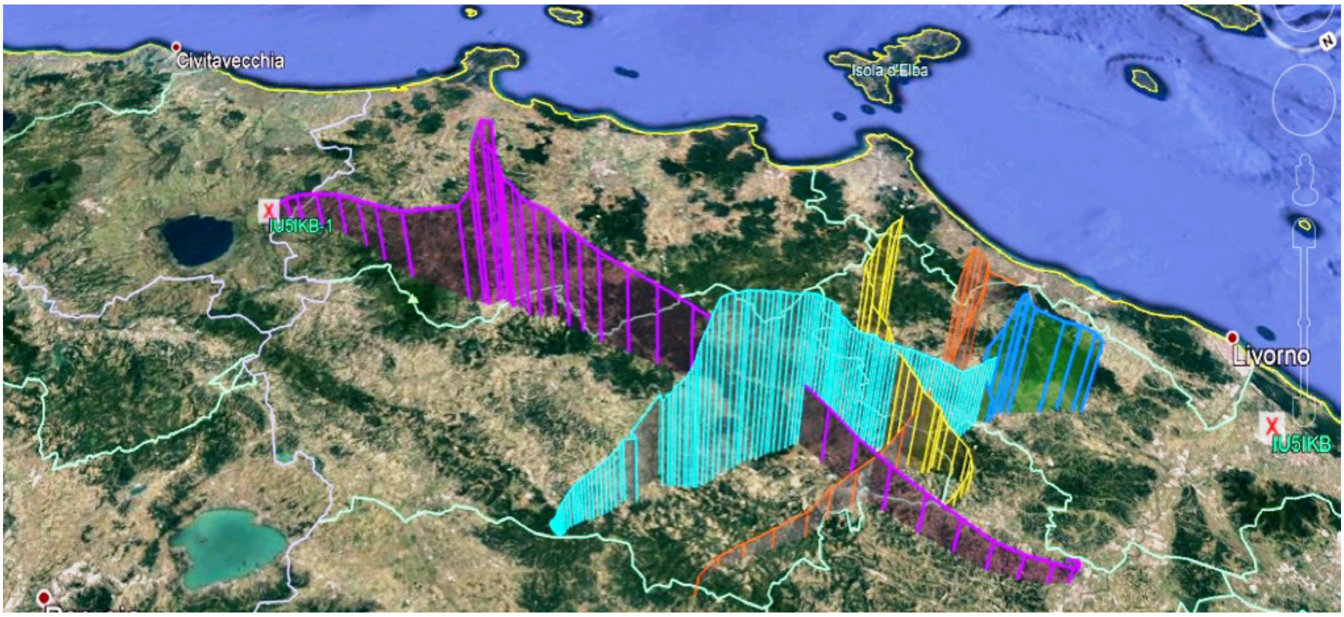

Figure 14 - ISM-HAB missions flight trajectories

3.2 MISSION PHASES

Each mission is composed of several phases, summarized in Figure 13. First, the HAB is released into the atmosphere from the launch site (1). Typically, the launch operations do not require more than five people. Then, the balloon starts the ascent phase (2) up to when it reaches its maximum size and bursts (3). From this moment on, the payload starts the descent phase (4) under parachute braking. Finally, the payload is recovered (5) by the chase team (0) and the several micro SD containing data collected by the various on-board system (RF payload and tracking systems) are recovered. The chase team relies both on the APRS data and the SPOT tracer position to follow the payload location during the flight.

The payload has never been lost during all of our ISM-HAB missions. The recovery procedure proved to be reliable and quick. Figure 14 shows the five ISM-HAB missions flown under this project; Table 2 summarizes the missions' key parameters.

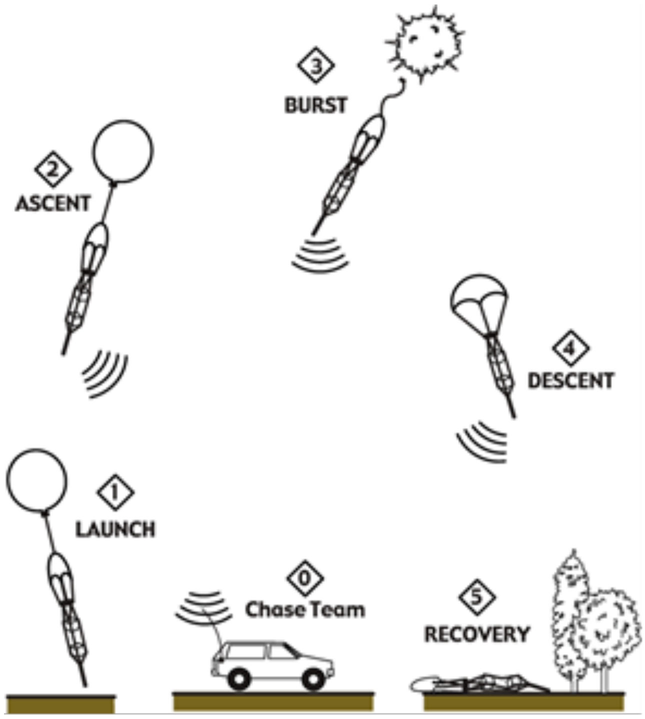

Figure 13 - Mission sequence

	ISM-HAB#1	ISM-HAB#2	ISM-HAB#3	ISM-HAB#4	ISM-HAB#5
Mission	Test launch w/o RF payload	2,4 GHz, DSA w/ sampling rate 1 MHz	2,4 GHz, DSA w/ sampling rate 1 MHz	868 MHz, DSA w/ sampling rate 100 KHz	2,4 GHz, DSA w/ sampling rate 100 KHz + SAMPLE RECORDING
Payload weight (w/o parachute) (g)	1450	1830	1840	1960	1960
Launch Date and Time	13/09/18 13:05	02/10/18 15:30	12/10/18 2:38	27/10/18 11:32	14/11/18 12:32
Launch site (City, District)	Lajatico (PI)	Montegonzi (AR)	Certaldo (FI)	Ponte a Elsa (FI)	Lajatico (PI)
Landing site (City, District)	Villamagna (PI)	Cecina (LI)	Monteguidi (SI)	Latera (VT)	Rapolano Terme (SI) -
Landing site (type)	Woods	Woods	Woods	Grassland	Woods
Payload Recovered	YES	YES	YES	YES	YES
Weather conditions	Cloudy	Rainy	Sunny	Sunny	Sunny
Peak Altitude [km]	21.038	19.115	32.412	30.400	29.493
Total Distance Covered [km]	8.3	78.3	28.8	137	74
Total Flight Time [min]	118	123	210	236	176
Ascent Time [min]	91	93	152	185	114
Descent Time [min]	27	30	58	51	62
Mean Ascent Velocity [m/s]	3.85	3.4	3.7	2.7	4.3
Mean Descent Velocity [m/s]	12.98	10.5	9.2	9.7	7.9
Landing Velocity [m/s]	9.9	6	5.3	3.4	3.4

Table 2 – Key Figures of the ISM-HAB Missions

4 DATA ANALYSIS

4.1 Vertical motion

As it can be seen from Figure 15, the rate of ascent of the balloons during all the missions was almost constant. This is believed to be due to the fact that while the balloon rises, the air becomes increasingly rarefied and its density drops. In the same way, the balloon expands, exposing a larger cross section. The two effects compensate each other so that the rising speed is almost constant; therefore, the ascent rate depends essentially on the amount of lift initially imposed on departure. If the weather is rainy or very cloudy the water and the ice that the payload will encounter during ascent may cause an early burst at an altitude of about 20 km instead of the nominal 30-35 km.

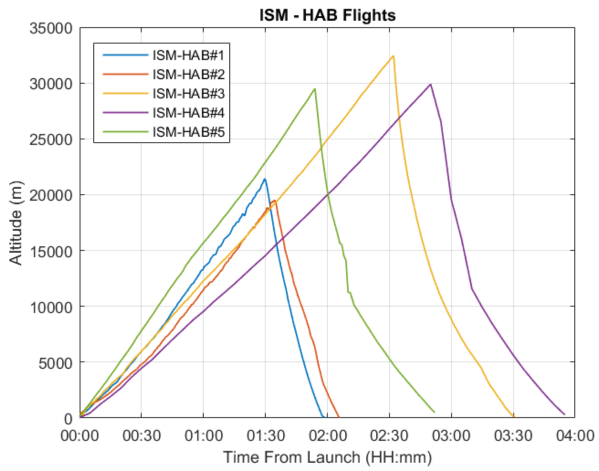

Figure 15 - ISM-HAB Missions Altitude Profile

Lower burst altitude means that the total distance traveled will be shorter, as happened with ISM-HAB#1 and ISM-HAB#2. If the burst happens too early, a larger portion of the balloon could remain attached to the payload, affect the correct deployment of the parachute; in such conditions, the payload will descend more rapidly.

Some difficulties in predicting the ascent rate were encountered. Specifically, as it can be seen in Figure 16, the simulator used to overpredict the ascent rate, imposing an initial lift mass. Having set different lifts for each mission, and having achieved different ascent rates, a relationship thanks to the fitting of the measured data was found (Fig.17). A new version of the PyLandingPredictor will implement this formula.

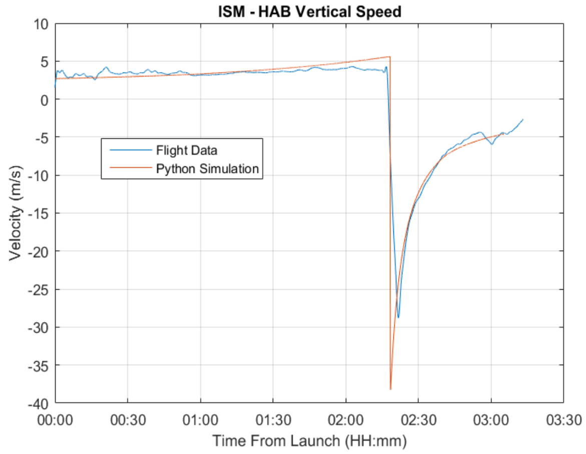

Figure 16 - ISM-HAB#3 Velocity simulation-real comparison

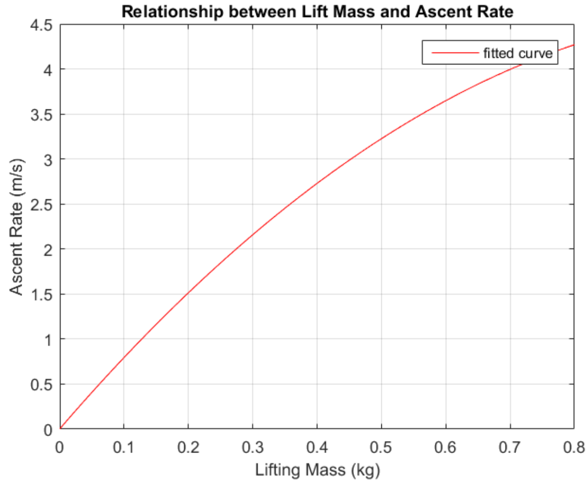

Figure 17 – Ascent rate as a function of lifting mass

4.2 Horizontal Motion

Most of the distance travelled by the payload is covered inside the troposphere, in which the strongest winds reside. This situation is clearly illustrated in Figure 18. These winds normally reach velocities of 80-90 km/h near 10 km altitude. This is something crucial for those who intend to perform HAB launches: with a limited amount of lift, the balloon will be subjected to these winds for a relatively long time, as it will reach his burst altitude very late. This will make it to travel for very long distances, thus reducing the likelyhood of its recovery. Therefore, it is strongly suggested

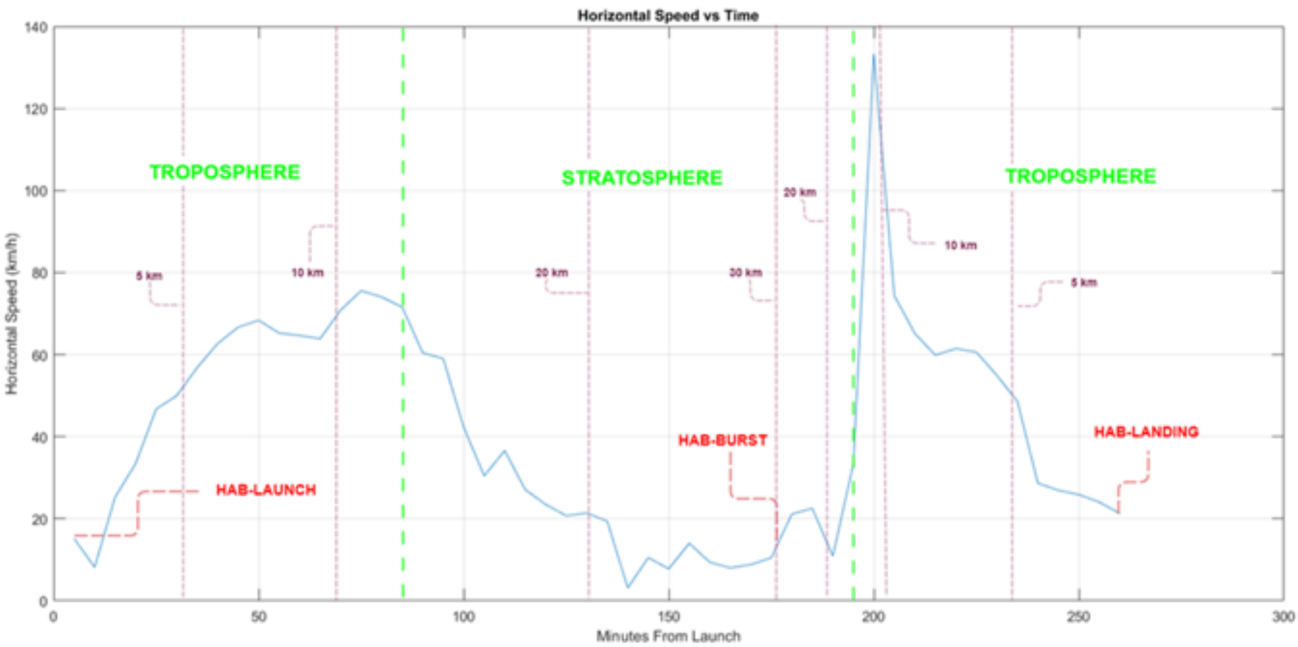

Figure 18 – ISM-HAB#3 Horizontal Speed

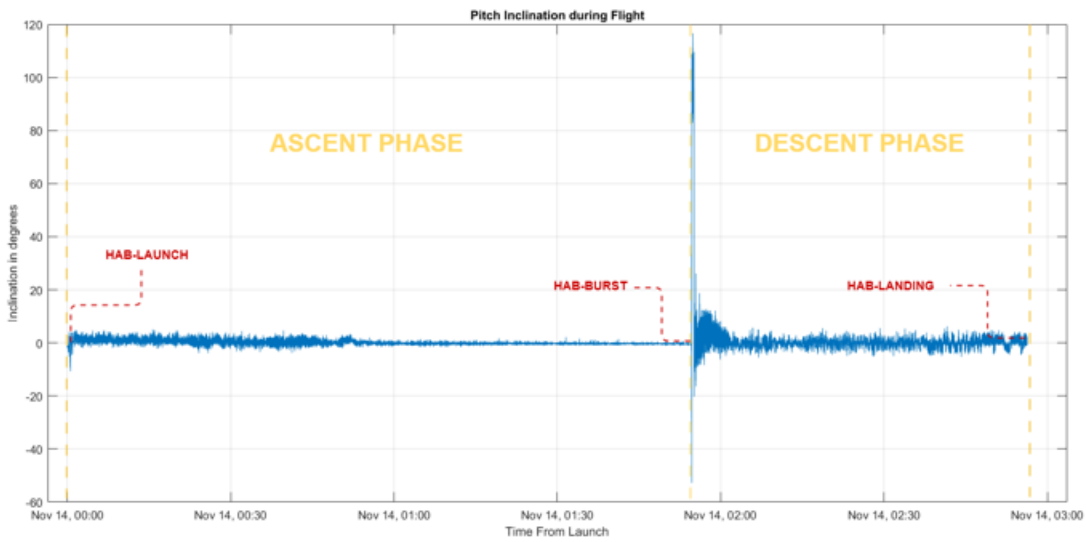

Figure 19 – Pitch oscillations registered by the IMU during ISM-HAB#3

to set about 0.5 kg of lift, so that the balloon will reach its burst altitude as quickly as possible. This will reduce not only the distance traveled to the landing site but also the mission duration, making it more likely that the payload is recovered on the same day of the launch.

4.3 Oscillations

While the balloon ascends, the payload is subjected to a variety of oscillations. Specifically, it oscillates around both pitch and roll axis while it rotates around its yaw axis, as per the reference system shown in Fig 2.

In order to have a clear understanding of its dynamics during the flight, an IMU (Inertial Measurement Unit) was installed on the payload. This contains an accelerometer combined with a gyroscope that collect information about pitch and roll oscillations, as well as a magnetometer used to determine the heading of the roll axis and the rotation around the yaw axis. As shown in Figure 19, the ascent phase is characterized by small oscillations, decreasing with the altitude, while the burst results in several upturns of the payload (this was also confirmed by the recorded videos). The descent is instead quite turbulent. Pitch and roll oscillations have a similar behaviour.

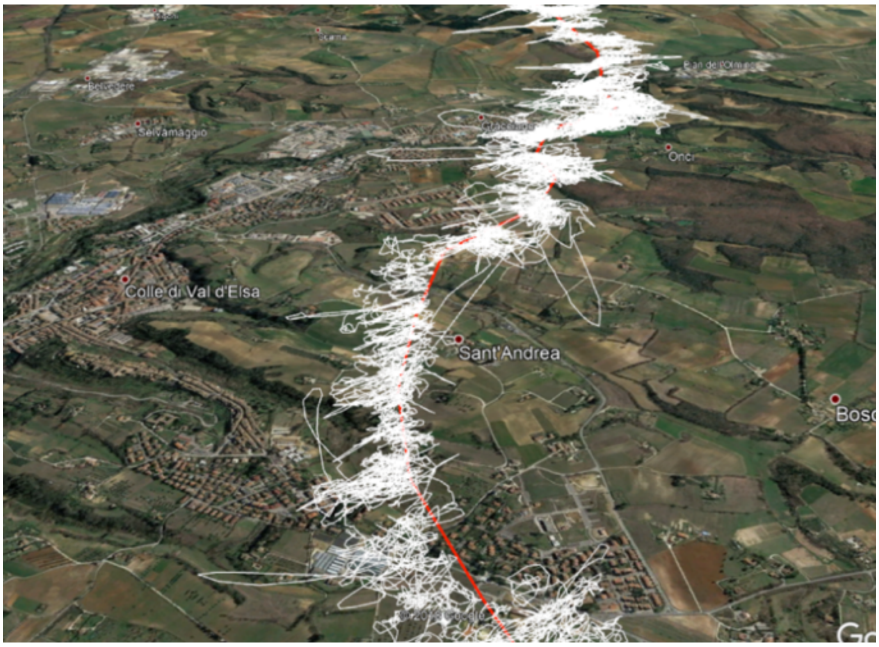

Figure 20 – Pointing path (white) and GPS positions (red)

Given the pitch, roll and yaw attitude angles measured by the IMU on the payload, the projected ground path seen by the bottom of the payload where the antenna was mounted could be reconstructed. To this end, a MATLAB script was written which computes the deviation from the local vertical from pitch and roll, then projects it in the appropriate direction (determined through the yaw measurement from the magnetometer), and finally outputs a KML file usable with Google Earth Pro. This procedure was requested by the project customer in order to have a precise understanding of where the antenna was pointing to during flight. An example is shown in Fig 20.

By making a Fourier analysis of the signal that represents the pitch oscillations it is clear that there are no clearly detectable characteristic frequencies in angular motion during the first phases of the ascent. At low altitudes the air turbulence produces a signal that is essentially random. On the contrary, in the stratosphere a characteristic frequency is clearly visible (Fig. 21). This frequency corresponds to the free oscillation of a pendulum in empty space with a cord length exactly equal to the distance between the payload and the balloon, i.e. 0.178 Hz.

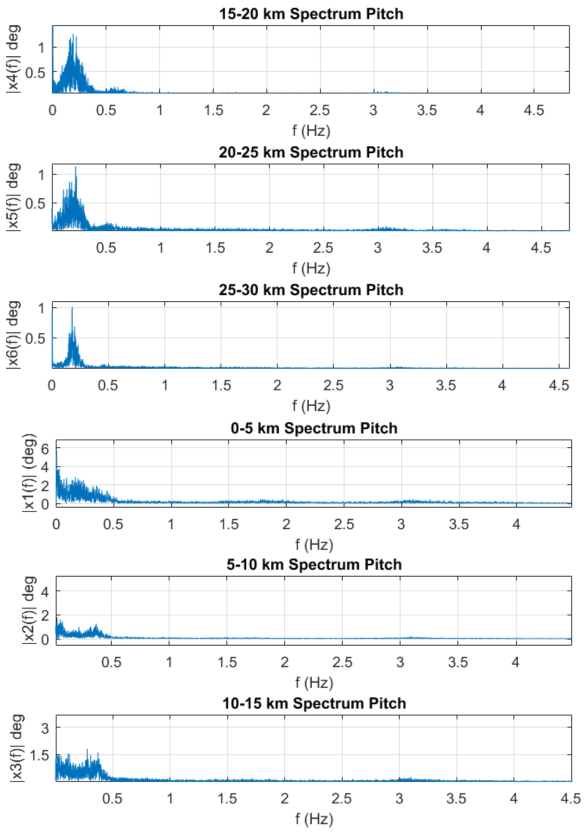

Figure 21 – Single sided amplitude spectrum pitch oscillations with increasing altitude (from top to bottom)

An attitude stabilization system would enhance the operational capability of the platform and make it well suited to a large variety of technology experiments of interest for future space missions. If such attitude stabilization is to be introduced, the most suitable phase of the mission for it would definitely be the one over 25 km altitude, where environmental torque disturbances are at a minimum and attitude stabilization could provide most effective. Figures 24 and 25 show the angular velocity and acceleration values computed during a time duration corresponding to transit of the blloon in between 25 to 30 km.

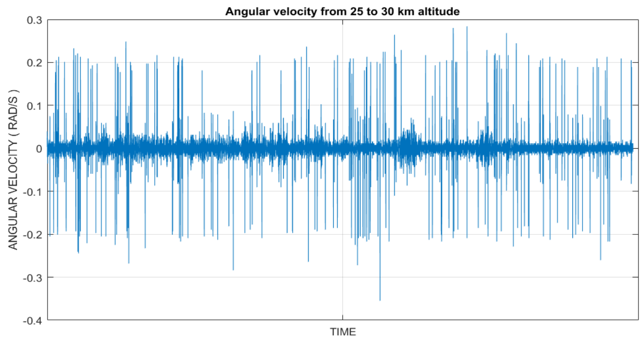

Figure 22 – Angular velocity from 25 to 30 km altitude

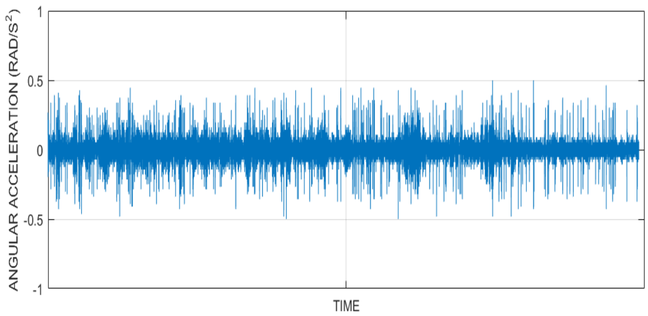

Figure 23 – Angular accelerations from 25 to 30 km altitude

4.4 Internal and external temperatures

Polystyrene proved to be a nice thermal insulating material. During all five ISM-HAB flights, the temperature inside the payload stayed between 30 °C and 52 °C while the outside temperature reached a minimum of - 46 °C. So, all the electronic components inside the payload were inside their operative temperature range. No active thermal control system was needed to warm the components because ground tests revealed that the RF components already developed a considerable amount of heat. In fact, after turning on the electric components and sealing the payload before the launch, the temperature inside the box increased

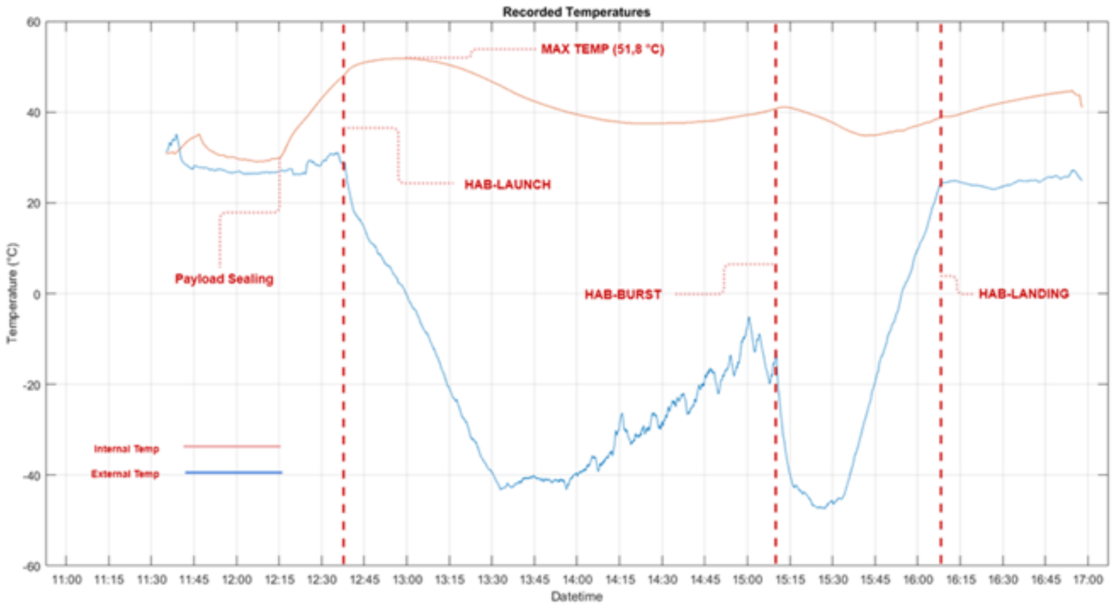

Figure 26 - ISM-HAB#3 Temperature measurement inside the polystyrene box (red curve) and outdoor (blue)

quite quickly. The measured temperatures and the relative graph are shown in Fig 26.

4.5 RF measurements

Figures 27 and 28 represent the spectrograms of the recorded signals, reported to the antenna connector output, respectively for the ISM 2.4 GHz band and for the 862-922 MHz band. The spectrograms show the spectral power density [dbm/MHz & DBM/100khz] of the ground-produced ISM noise that was measured during the HAB flights.

As it can be seen from the spectrograms, some frequency ranges are characterized by the near-absence of interferent emissions, while others are associated with relatively high RF power. In particular, no significant emissions have been recorded in the band 900-917 MHz (US-licensed band) and in the band 2.485-2.5 GHz, of common use in Europe. Such s]ub-intervals of the ISM bands are therefore suited for a dedicated IoT application making use of LEO satellite without little or no risk of being affected by ground-genersated interference.

The interferences measured at 32 km can be appropriately scaled via software in order to estimate the interferences collected by a spacecraft in orbit at an altitude of 600 km (as in a typical LEO small satelliyte mission). This provides useful indications for the design of a future IoT constellation in LEO.

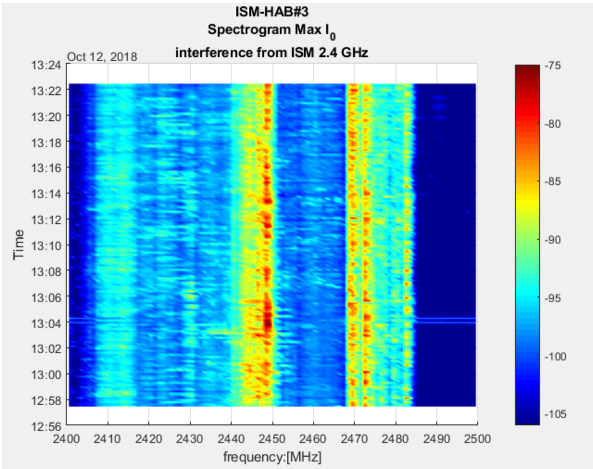

Figure 27 – ISM 2.4 GHz interference spectrogram

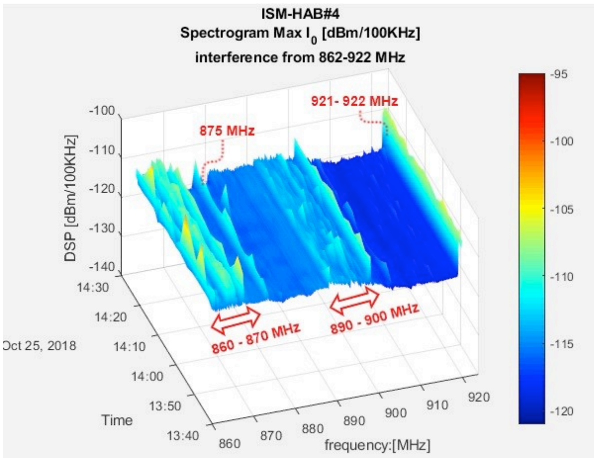

Figure 28 – ISM 862-922 MHz interference spectrogram

5 CONCLUSIONS AND FUTURE WORK

The five ISM-HAB missions flown can be considered a success. Valuable data regarding the interference measurements and the dynamics of the balloon were obtained. All this has been done thanks to the work of a few people, with relatively cheap and easy to find components. The payload was easily readjusted and updated between one mission and the other. Therefore, it has been shown that this platform concept is particularly suitable for TLC-type research. However, the need to recover the payload without being able to access the data in real time during flights remains a limitation of this technology.

A first attempt to characterize the dynamic environment was made. For the future, we plan to continue to collect this kind of data, perhaps using inertial sensors of better sensitivity and accuracy. The ultimate goal is the design and realization of a payload attitude stabilization system for the high altitude portion of the flight. With such a feature, the possibilities of this platform might extend also to other research areas such as astronomy and Earth imaging. Moreover, the provision of attitude stabilization would enable the realization of inter-HAB laser links between multiple balloons, so to simulate inter-satellite optical links in a very realistic way at low cost.

Acknowledgments

This work was carried out in the frame of a collaboration between Eutelsat SA, MBI Srl and two Departments of the University of Pisa (DII-Information Engineering and DICI-Aerospace Division). The author gratefully acknowledges the help of Ing. Marco Andrenacci, Attilio Vaccaro, Michele Gammone, Leonardo Nanna of MBI and Prof. Salvo Marcuccio of Università di Pisa.

References

1. http://news.eutelsat.com/pressreleases/eutelsat-commissions-elo-its-first-low-earth-orbit-satellite-designed-for-the-internet-of-things-2440770

2. https://www.thinxtra.com/2018/08/sigfox_sensum_space/

3. https://www.researchgate.net/publication/323851404_Laboratory_testing_of_LoRa_modulation_for_CubeSat_radio_communications

4. https://www.aukey.com/products/pb-n28-12000mah-aipower-power-bank

5. https://en.wikipedia.org/wiki/Automatic_Packet_Reporting_System

6. https://cdn.shopify.com/s/files/1/0277/1287/files/StratoTrack_User_Guide_V1.0.pdf?10561192249952171327

7. https://www.globalstar.com/en-gb/products/spot/spot-trace

8. https://www.highaltitudescience.com/products/eagle-flight-computer

9. http://ozzmaker.com/wp-content/uploads/2017/11/LSM9DS1.pdf

10. https://www.raspberrypi.org/products/raspberry-pi-zero/

11. Luke W. Renegar, "A Survey of Current Balloon Trajectory Prediction Technology", 2017 Academic High Altitude Conference, University of Minnesota - Twin Cities, 2017. https://via.library.depaul.edu/ahac/2017/poster2/3/

12. Travis Fields, Milan Heninger, Jeffrey LaCombe, Eric Wang, "In-flight Landing Location Predictions using Ascent Wind Data for High Altitude Balloons", AIAA Balloon Systems (BAL) Conference, 2013. doi: 10.2514/6.2013-1294

13. Rodger E. Farley, "BalloonAscent: 3-D Simulation Tool for the Ascent and Float of High-Altitude Balloons", AIAA 2005-7412, 5th ATIO and 16th Lighter-Than-Air Sys Tech. and Balloon Systems Conferences, Arlington, Virginia, 2005. doi: 10.2514/6.2005-7412

14. A. Gallice, F. G. Wienhold, C. R. Hoyle, F. Immler, and T. Peter, "Modeling the ascent of sounding balloons: derivation of the vertical air motion", Atmos. Meas. Tech., 4, 2235-2253, 2011. doi: 10.5194/amt-4-2235-2011

15. Timothy Paul Smith, "Balloon Calculations". Retrieved from http://northstar-www.dartmouth.edu/~klynch/pmwiki-gc/uploads/BalloonCalulations.pdf

16. https://www.ready.noaa.gov/READYcmet.php